

We are IntechOpen, the world's leading publisher of Open Access books Built by scientists, for scientists

6,900

Open access books available

186,000

International authors and editors

200M

Downloads

Our authors are among the

154

Countries delivered to

TOP 1%

most cited scientists

12.2%

Contributors from top 500 universities



WEB OF SCIENCE™

Selection of our books indexed in the Book Citation Index
in Web of Science™ Core Collection (BKCI)

Interested in publishing with us?
Contact book.department@intechopen.com

Numbers displayed above are based on latest data collected.
For more information visit www.intechopen.com



Controlling Equilibrium and Synchrony in Arrays of FitzHugh–Nagumo Type Oscillators

Elena Adomaitienė, Skaidra Bumelienė and
Arūnas Tamaševičius

Additional information is available at the end of the chapter

<http://dx.doi.org/10.5772/intechopen.74337>

Abstract

We present a case study of the FitzHugh–Nagumo (FHN) type model with a strongly asymmetric activation function. The proposed model is an electronically rather than a biologically inspired approach. The asymmetric exponential model imitates the shape of spikes in real neurons better than the classical FHN model with a cubic van der Pol activation function. An array of mean-field coupled non-identical FHN type oscillators is considered. The effect of mutual synchronization (phase locking) of units, originally oscillating at their individual frequencies, is demonstrated. Several feedback control methods, including stable tracking filter technique, mean field nullifying, and repulsive coupling are shown either to stabilize unstable equilibrium states or to suppress synchrony of the coupled FHN oscillators. The stability of the equilibrium states is analyzed by employing the eigenvalues, obtained from the characteristic equation, and by using the diagonal minors of the Routh–Hurwitz matrix. Nonlinear differential equations are solved numerically.

Keywords: nonlinear dynamics, spiking neuron model, FitzHugh–Nagumo oscillator, arrays of coupled oscillators, equilibrium states, synchronization, control methods

1. Introduction

The stability of any either natural or artificial system is a valuable and desired property. Therefore, the control of dynamical systems, in particular stabilization of their unstable equilibrium (UEQ) states, is an important problem in basic science and engineering applications, if periodic or chaotic oscillations are unacceptable behaviors. Usual control methods, based on proportional feedback control [1, 2] require knowledge of a mathematical model of a

dynamical system or at least the exact coordinates of the UEQ in the phase space for the reference point. However, in many real complex systems, especially in biology, physiology, economics, sociology, and chemistry neither the full reliable models nor the exact coordinates of the UEQ are a priori known. Moreover, the position of the UEQ may change with time because of external unknown and unpredictable forces. In these cases, adaptive, that is model-independent and reference-free methods, automatically tracing and stabilizing unknown UEQ, can be helpful [3–5].

Synchronization is a universal and very common phenomenon, widely observed in nature, science, engineering, and social life [6]. Coupled oscillators and their arrays, exhibiting synchrony, range from pendulum clocks to various biological populations. In many cases, synchronization plays a positive role. However, sometimes, it has an unfavorable impact. Strong synchronization of neurons in human brain is an example. It is assumed that synchrony of spiking neurons in a neuronal population causes the symptoms of the Parkinson's disease and essential tremor [7]. Therefore, development of the methods and practical techniques for controlling, more specifically, for suppressing synchrony of coupled oscillators, in general, and particularly with possible application to neuronal arrays, is of great importance [8–10].

A variety of adaptive feedback methods for stabilizing UEQ of nonlinear dynamical systems have been described in literature. Here, we mention only some of them, e.g., derivative control technique [11–13], stable filter technique [3, 4, 14–17], unstable filter technique [18–20], and combined filters techniques [21–23]. A comprehensive list and an overview of control methods developed to stabilize UEQ states can be found in [24]. We note that the above mentioned techniques deal with single unstable dynamical systems. Stabilization of a network of coupled oscillators has been considered in a recent paper [25].

Suppression of synchrony in arrays of oscillators by means of feedback methods has been described in many papers [7–10, 26–29]. More publications and discussion on the feedback techniques for control of synchrony are presented in [24, 25].

Another way to avoid synchrony in arrays of oscillators is a non-feedback method using external periodic drive at relatively high frequency (much higher than the natural frequency of the oscillators). In neurology, it is known as deep brain stimulation (DBS), applying about 150 Hz periodic pulses to certain brain areas [30]. It is a clinically approved therapy for patients with the Parkinson's disease symptoms. However, mechanism of the DBS is not fully understood. There are several papers considering the Hodgkin–Huxley and the FitzHugh–Nagumo models and demonstrating that high frequency forcing can stabilize the UEQ of the neuronal oscillators and thus inhibit spiking cells [31–33].

In this chapter, we present a case study of the FitzHugh–Nagumo (FHN) type model with a strongly asymmetric activation function (Section 2). An array of mean-field coupled non-identical FHN type oscillators is considered in Section 3. The effect of mutual synchronization (phase locking) of units originally oscillating at their individual frequencies is demonstrated. Several feedback control methods, including stable tracking filter technique (Section 4), mean field nullifying (Section 5), and repulsive coupling (Section 6) are shown either to stabilize UEQ states or to suppress synchrony of the coupled FHN type oscillators.

2. Single FHN type oscillator

An extremely simple electrical circuit, imitating a single spiking neuron, is sketched in **Figure 1**. The negative resistance R_n can be implemented by means of a negative impedance converter [34]. Typical train of spikes from its output is presented in **Figure 2**.

We apply the Kirchhoff's laws to electrical circuit in **Figure 1**, use the Shockley current–voltage characteristic for the diode, and introduce the following dimensionless quantities:

$$x = \frac{V_C}{V^*}, \quad y = \frac{\rho I_L}{V^*}, \quad t \rightarrow \frac{t}{\sqrt{LC}}, \quad \alpha = \frac{\rho}{|R_n|}, \quad \beta = \frac{r}{\rho}, \quad \gamma = \frac{I\rho}{V^*}, \quad \delta = \frac{I_S\rho}{V^*}, \quad \mu = \frac{qV^*}{nk_B T}, \quad \rho = \sqrt{\frac{L}{C}} \quad (1)$$

where $V^* = 1$ V, k_B is the Boltzmann constant, T is the absolute temperature (in K), q is the elementary charge, $k_B T/q$ is the thermal potential (≈ 25 mV at room temperature, $T = 293$ K), n is a diode ideality factor, sometimes called emission coefficient (assumed value $n = 2$). Then, differential equations, convenient for analysis and numerical integration, are derived:

$$\begin{aligned} \dot{x} &= F(x) - y - \gamma, \\ \dot{y} &= x - \beta y. \end{aligned} \quad (2)$$

Activation function $F(x)$ in Eq. (2) is a strongly asymmetric one (**Figure 3**):

$$F(x) = \alpha x + \delta [\exp(-\mu x) - 1]. \quad (3)$$

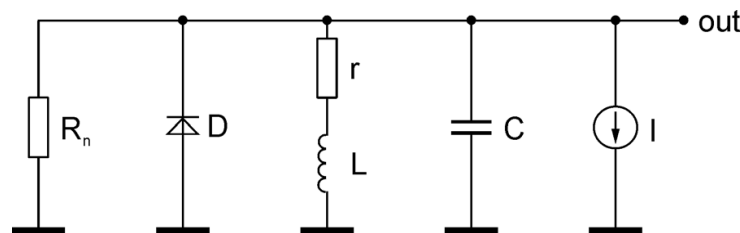


Figure 1. Circuit diagram of the electronic analog of spiking neuron. R_n is a negative resistance.

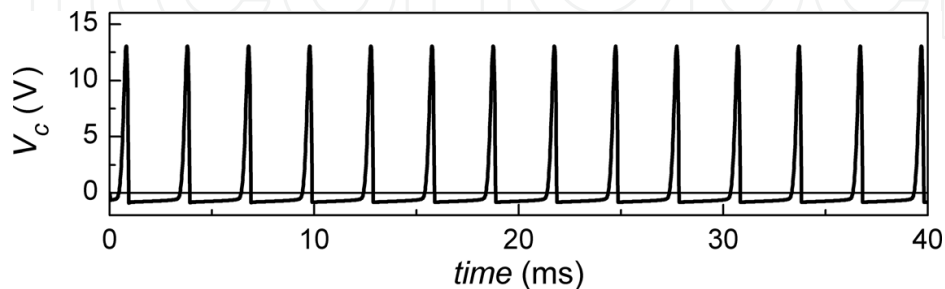


Figure 2. Voltage spikes from the circuit in Figure 1, generated by means of Electronics Workbench Professional software. $R_n = -680 \Omega$, D is a semiconductor diode (BAV99 type) with saturation current $I_S = 10$ nA ($\delta = 10^{-5}$), $L = 100$ mH, $C = 100$ nF, ($\rho = 1$ k Ω), $r = 50 \Omega$ ($\beta = 0.05$), $I = 1$ mA ($\gamma = 1$).

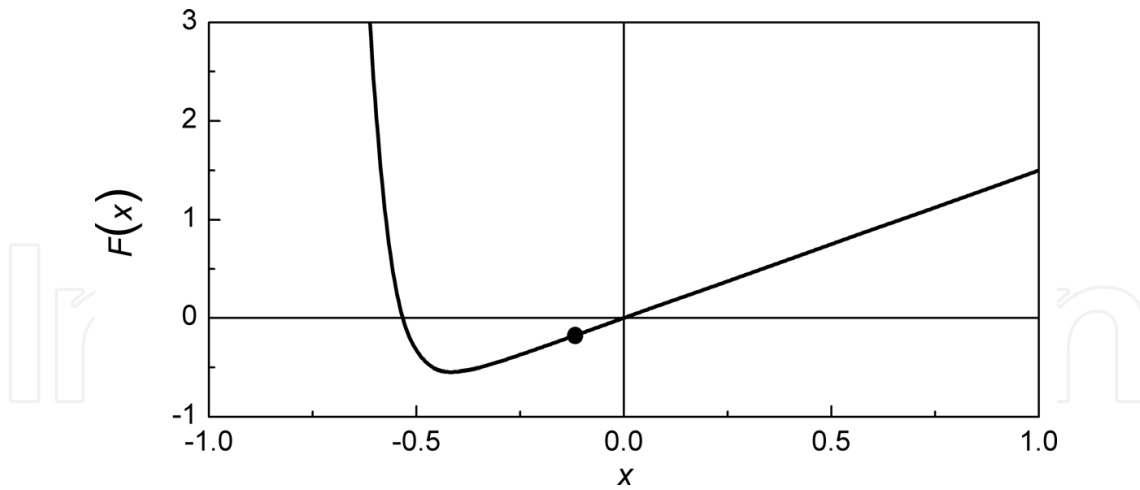


Figure 3. Activation function $F(x)$ from formula (3). $\alpha = 1.5$, $\delta = 10^{-5}$, and $\mu = 20$. Black dot on the curve marks the equilibrium coordinate $x_0 = -0.12$ from formula (5) at $\beta = 0.1$ and $\gamma = 1$.

$F(x)$ essentially differs from the odd function $F_{\text{FH}}(x) = x - x^3/3$, introduced by FitzHugh [35] and used in many later papers, e.g., in [28]. It also differs from the asymmetric three-segment $[x < -1, -1 \leq x \leq 1, x > 1]$ piecewise linear function $F_{\text{PL}}(x) = \alpha x + d(x+1)H(-x-1) + g(x-1)H(x-1)$ suggested in [36], where $d \gg g$ and $H(u)$ is the Heaviside unit step function, i.e., $H(u > 0) = 1$, $H(u \leq 0) = 0$. In contrast to the $F_{\text{PL}}(x)$, the $F(x)$ is a smooth function, and therefore it seems a more realistic option.

For $\alpha\beta < 1$ and

$$\gamma \ll \frac{1 - \alpha\beta}{\mu\beta} \ln \delta^{-1} \quad (4)$$

the equilibrium solution of Eq. (2) is given by the fixed point coordinates

$$x_0 = -\frac{\beta\gamma}{1 - \alpha\beta}, \quad y_0 = -\frac{\gamma}{1 - \alpha\beta}. \quad (5)$$

Due to the exponent in the activation function $F(x)$, strong inequality (4) practically can be replaced with a simple inequality:

$$\gamma \leq \frac{1 - \alpha\beta}{2\mu\beta} \ln \delta^{-1}. \quad (6)$$

Note empiric factor 2 is in the denominator. Eqs. (2), linearized around the fixed point (5), read

$$\begin{aligned} \dot{x} &= \alpha x - y, \\ \dot{y} &= x - \beta y. \end{aligned} \quad (7)$$

The corresponding characteristic equation is

$$\lambda^2 - (\alpha - \beta)\lambda + 1 - \alpha\beta = 0. \quad (8)$$

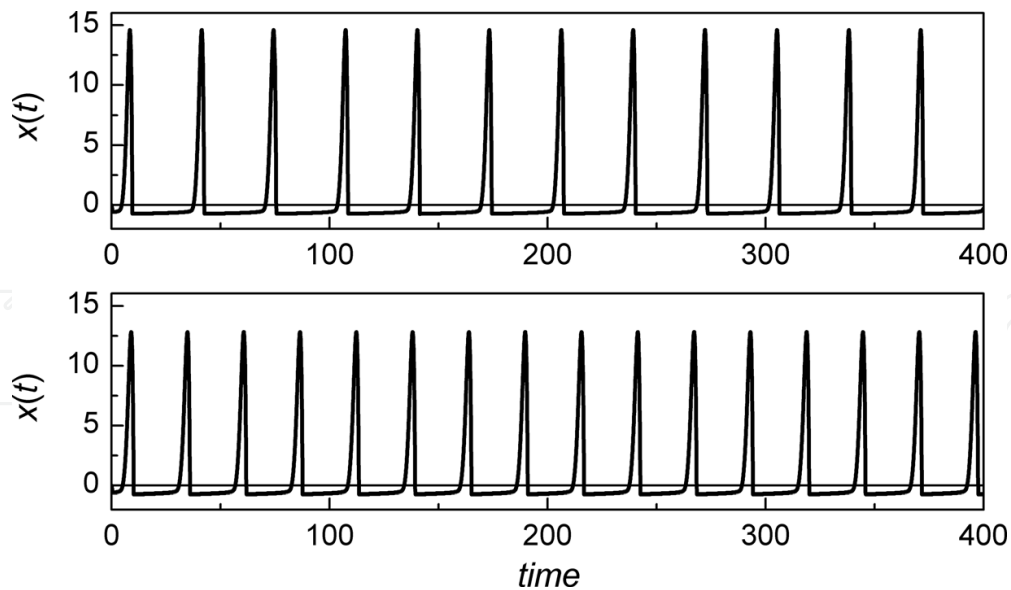


Figure 4. Waveforms $x(t)$ from Eq. (2) with $\alpha = 1.5$, $\gamma = 1$, $\delta = 10^{-5}$, and $\mu = 20$ for different damping β . (Top) $\beta = 0.05$ and (bottom) $\beta = 0.1$. Note, different inter-spike periods in the two plots.

It has two eigenvalues

$$\lambda_{1,2} = \frac{(\alpha - \beta)}{2} \pm \sqrt{\frac{(\alpha - \beta)^2}{4} - (1 - \alpha\beta)} = \frac{(\alpha - \beta)}{2} \pm \sqrt{\frac{(\alpha + \beta)^2}{4} - 1}. \quad (9)$$

If $\alpha > \beta$, then both real parts of the eigenvalues, $\text{Re}\lambda_{1,2}$ are positive, proving that the equilibrium (x_0, y_0) is an unstable fixed point. If $\alpha + \beta > 2$, it is a node, and if $\alpha + \beta < 2$, it is a spiral.

Numerical solution of nonlinear equation Eq. (2) is presented in **Figure 4**.

3. Array of FHN type oscillators

An array of isolated (non-coupled) oscillators is given by

$$\begin{aligned} \dot{x}_i &= F(x_i) - y_i - \gamma, \\ \dot{y}_i &= x_i - \beta_i y_i, \end{aligned} \quad (10)$$

$$F(x_i) = \alpha x_i + \delta [\exp(-\mu x_i) - 1]. \quad (11)$$

Here and elsewhere $i = 1, 2, \dots, N$. Note that the structure of function $F(x)$ and parameters α , δ , and μ are the same for all oscillators, whereas the damping parameters β_i in Eq. (10) are intentionally set different for each oscillator to make them slightly non-identical units.

Now we introduce interaction between oscillators. To be specific, we consider mean-field coupling, which is also called “star” coupling in electronics (**Figure 5**):

$$\begin{aligned} \dot{x}_i &= F(x_i) - y_i - \gamma + k(\langle x \rangle - x_i), \\ \dot{y}_i &= x_i - \beta_i y_i \end{aligned} \tag{12}$$

Here, $k = \rho/R^*$ is the strength of coupling and

$$\langle x \rangle = \frac{1}{N} \sum_{i=1}^N x_i. \tag{13}$$

Typical phase portraits for isolated and coupled (synchronized) oscillators are shown in **Figure 6**. Intricate phase trajectories in **Figure 6 (left)** indicate that the oscillators are not synchronized, but oscillate at their individual frequencies, whereas simple closed loop in **Figure 6 (right)**

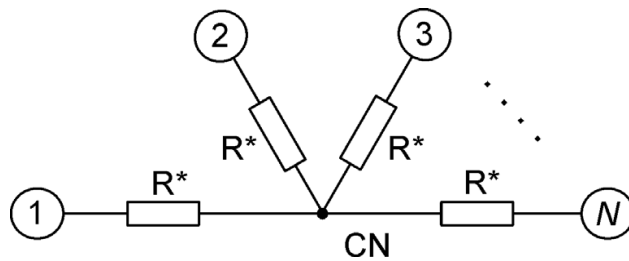


Figure 5. Diagram of mean-field coupled oscillators. R^* are coupling resistors and CN is a coupling node.

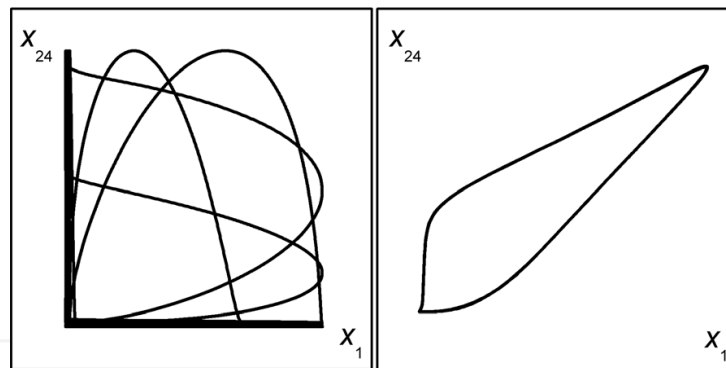


Figure 6. Phase portraits. $N = 24$, $\alpha = 1.5$, $\beta_i = 0.05 + 0.001i$, $\gamma = 1$, $\delta = 10^{-5}$, and $\mu = 20$. (Left) Isolated oscillators either from Eq. (10) or Eq. (12) with $k = 0$, and (right) coupled oscillators from Eq. (12) with $k = 1$.

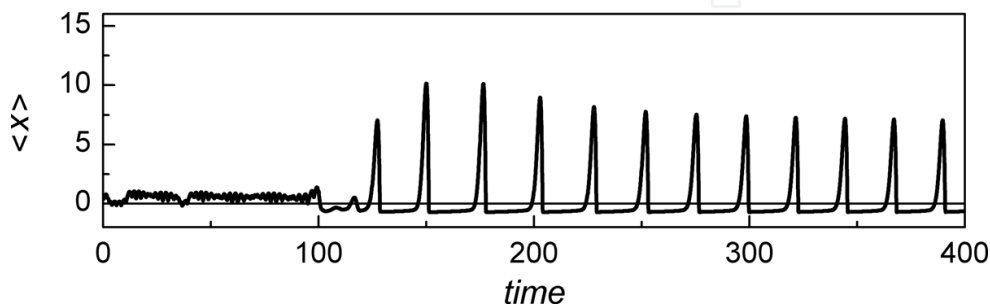


Figure 7. Waveform of the mean-field variable $\langle x \rangle$ from Eq. (12). $N = 24$, $\alpha = 1.5$, $\beta_i = 0.05 + 0.001i$, $\gamma = 1$, $\delta = 10^{-5}$, and $\mu = 20$. Coupling ($k = 1$) is switched on at $t = 100$.

proves that oscillators are in synchrony (phase-locked), i.e., oscillate at the same frequency. For synchronized oscillators, the phase difference is not necessarily zero (the phase portrait is not fine diagonal), but it does not change with time. The mean variable $\langle x \rangle$ for the two cases is shown in **Figure 7**. The amplitude of mean-field variable $\langle x \rangle$ is relatively low for isolated oscillators ($k = 0$), but becomes large for synchronized state ($k = 1$).

4. Stabilizing equilibrium states in array of oscillators

When an external capacitor is applied to the coupling node CN (**Figure 8**), the overall system becomes $(2N + 1)$ -dimensional system:

$$\begin{aligned} \dot{x}_i &= F(x_i) - y_i - \gamma + k(z - x_i), \\ \dot{y}_i &= x_i - \beta_i y_i, \\ \dot{z} &= \omega_f (\langle x \rangle - z). \end{aligned} \tag{14}$$

Here, z is a dimensionless dynamical variable related to voltage across the external capacitor C_0 , $z = V_{C_0}/V^*$, the mean $\langle x \rangle$ is given by formula (13), and ω_f is the dimensionless cut-off frequency of the filter composed by R^* and C_0 .

Analysis of the high-dimensional system is very complicated. Therefore, we consider a mean-field approach. We average all terms in Eq. (14) over all oscillators $i = 1, 2, \dots, N$:

$$\begin{aligned} \langle \dot{x} \rangle &= \langle F \rangle - \langle y \rangle - \gamma + k(z - \langle x \rangle), \\ \langle \dot{y} \rangle &= \langle x \rangle - \langle \beta y \rangle, \\ \dot{z} &= \omega_f (\langle x \rangle - z). \end{aligned} \tag{15}$$

Here,

$$\langle x \rangle = \frac{1}{N} \sum_{i=1}^N x_i, \quad \langle y \rangle = \frac{1}{N} \sum_{i=1}^N y_i, \quad \langle F \rangle = \frac{1}{N} \sum_{i=1}^N F(x_i), \quad \langle \beta y \rangle = \frac{1}{N} \sum_{i=1}^N \beta_i y_i, \quad \omega_f = \frac{N\sqrt{LC}}{R^*C_0}. \tag{16}$$

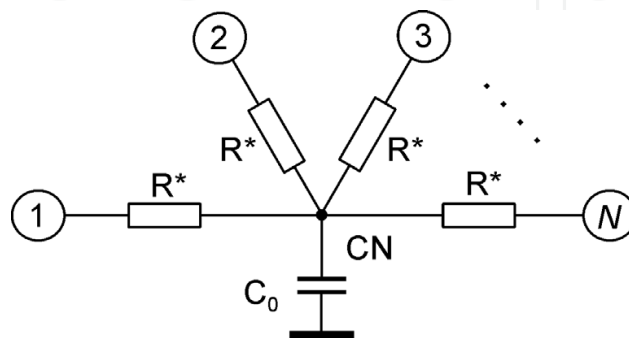


Figure 8. Diagram of mean-field coupled oscillators with a stabilizing capacitor C_0 . Stable RC filter is composed of coupling resistors R^* and capacitor C_0 (see formulas (16)).

Eq. (15) is not suitable to describe full dynamics of the system. However, we can exploit it to find equilibrium coordinates. If inequality (6) is valid for all oscillators with different β_i , the steady-state equations read

$$\begin{aligned} 0 &= \langle x_0 \rangle - \langle y_0 \rangle - \gamma + k(z_0 - \langle x_0 \rangle), \\ 0 &= \langle x_0 \rangle - \langle \beta y_0 \rangle, \\ 0 &= \langle x_0 \rangle - z_0. \end{aligned} \quad (17)$$

Here,

$$\langle x_0 \rangle = \frac{1}{N} \sum_{i=1}^N x_{0i}, \quad \langle y_0 \rangle = \frac{1}{N} \sum_{i=1}^N y_{0i}, \quad \langle \beta y_0 \rangle = \frac{1}{N} \sum_{i=1}^N \beta_i y_{0i}, \quad \langle \beta \rangle = \frac{1}{N} \sum_{i=1}^N \beta_i. \quad (18)$$

There is a problem in Eq. (17) with the term $\langle \beta y_0 \rangle$. In general, $\langle \beta y_0 \rangle \neq \langle \beta \rangle \langle y_0 \rangle$. However, if the ranges of the multiplicands β_i and y_{0i} in (18) are considerably different (in our case, the individual equilibrium coordinates y_{0i} in comparison with β_i , much weaker depend on i), then $\langle \beta y_0 \rangle \approx \langle \beta \rangle \langle y_0 \rangle$. Similarly to a single oscillator, considered in Section 2, for $\alpha \beta_i < 1$, the equilibrium coordinates are

$$\langle x_0 \rangle = -\frac{\langle \beta \rangle \gamma}{1 - \alpha \langle \beta \rangle}, \quad \langle y_0 \rangle = -\frac{\gamma}{1 - \alpha \langle \beta \rangle}, \quad z_0 = \langle x_0 \rangle. \quad (19)$$

Linearization of Eqs. (15) around the equilibrium coordinates yields:

$$\begin{aligned} \langle \dot{x} \rangle &= \alpha \langle x \rangle - \langle y \rangle + k(z - \langle x \rangle), \\ \langle \dot{y} \rangle &= \langle x \rangle - \langle \beta \rangle \langle y \rangle, \\ \dot{z} &= \omega_f (\langle x \rangle - z). \end{aligned} \quad (20)$$

The corresponding characteristic equation is

$$\lambda^3 + h_2 \lambda^2 + h_1 \lambda + h_0 = 0, \quad (21)$$

where

$$h_2 = -\alpha + \langle \beta \rangle + k + \omega_f, \quad h_1 = 1 - \alpha \langle \beta \rangle + \langle \beta \rangle k - (\alpha - \langle \beta \rangle) \omega_f, \quad h_0 = (1 - \alpha \langle \beta \rangle) \omega_f. \quad (22)$$

Numerical solution of Eq. (21) is presented in **Figure 9** for different values of the coupling parameter k . The equilibrium is stable, if the real parts of all three eigenvalues are negative, $\text{Re} \lambda_{1,2,3} < 0$.

Necessary and sufficient conditions of stability can be found analytically from the Hurwitz matrix

$$H = \begin{pmatrix} h_2 & h_0 & 0 \\ 1 & h_1 & 0 \\ 0 & h_2 & h_0 \end{pmatrix}. \quad (23)$$

The Routh–Hurwitz stability criterion claims that the system is stable, if all diagonal minors of the matrix H are positive:

$$\Delta_1 = h_2 > 0, \quad \Delta_2 = h_2 h_1 - h_0 > 0, \quad \Delta_3 = h_0 \Delta_2 > 0. \quad (24)$$

The first minor is $\Delta_1 > 0$, if

$$k > k_1 = \alpha - \langle \beta \rangle - \omega_f. \quad (25)$$

For $\alpha = 1.5$, $\beta_i = 0.05 + 0.001i$, and $\omega_f = 0.1$, the threshold is $k_1 = 1.34$.

The second minor Δ_2 is more cumbersome and yields quadratic equation:

$$\langle \beta \rangle k^2 + dk + g = 0. \quad (26)$$

where

$$\begin{aligned} d &= 1 - 2\alpha \langle \beta \rangle + \langle \beta \rangle^2 - (\alpha - 2\langle \beta \rangle)\omega_f, \\ g &= -(\alpha - \langle \beta \rangle) \left[1 - \alpha \langle \beta \rangle - (\alpha - \langle \beta \rangle)\omega_f + \omega_f^2 \right]. \end{aligned} \quad (27)$$

Eq. (26) has an analytical solution

$$k_{2,3} = -\frac{d}{2\langle \beta \rangle} \pm \sqrt{\frac{d^2}{4\langle \beta \rangle^2} - \frac{g}{\langle \beta \rangle}}, \quad (28)$$

which provides two different values. For $\alpha = 1.5$, $\beta_i = 0.05 + 0.001i$, and $\omega_f = 0.1$, the values are $k_2 = 1.44$ and $k_3 = -12.3$. Eventually, we evaluate the threshold $k_{th} = \max(k_1, k_2, k_3) = 1.44$. It is in a very good agreement with numerical value of k_{th} obtained from $\text{Re}\lambda_{1,2,3}(k)$ in **Figure 9**.

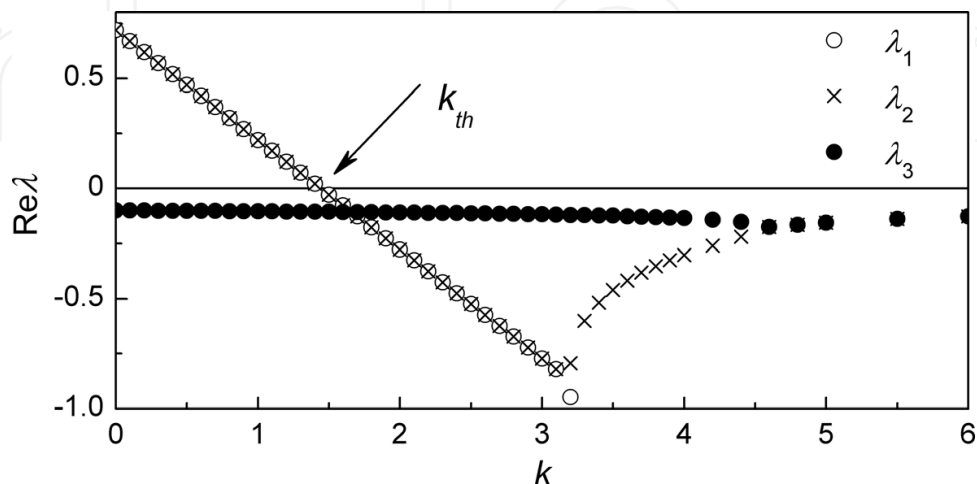


Figure 9. Real parts of the eigenvalues from Eq. (21). $N = 24$, $\alpha = 1.5$, $\beta_i = 0.05 + 0.001i$, $\langle \beta \rangle = 0.0625$, and $\omega_f = 0.1$. Arrow in the plot indicates the threshold coupling parameter $k_{th} = 1.44$, where the largest eigenvalues become negative.

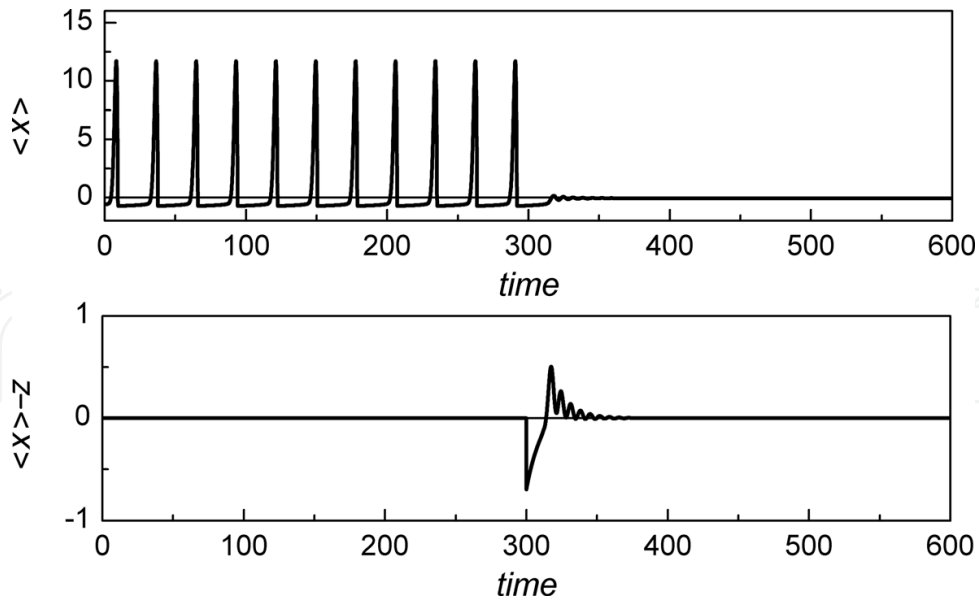


Figure 10. Waveforms from Eq. (14). $N = 24$, $\alpha = 1.5$, $\beta_i = 0.05 + 0.001i$, $\gamma = 1$, $\delta = 10^{-5}$, $\mu = 20$, $\omega_f = 0.1$, and $k = 1.6$. (Top) Mean-field variable $\langle x \rangle$, (bottom) control term $z - \langle x \rangle$. Control is switched on at $t = 300$ ($\langle x \rangle$ in the coupling term is replaced with z).

Once $\Delta_2 > 0$, the inequality for the third minor $\Delta_3 > 0$ can be replaced simply with $h_0 > 0$. This can be further simplified to $(1 - \alpha \langle \beta \rangle) > 0$, since $\omega_f > 0$ by definition. Finally, we come to inequality $\alpha \langle \beta \rangle < 1$, which satisfied by itself, because it was already used as an assumption to derive the equilibrium coordinates; see formulas (19).

Numerical results from Eqs. (14), demonstrating dynamics of equilibrium stabilization, are presented in **Figure 10**.

5. Mean-field “nullifying” technique

A straightforward way to desynchronize the mean-field coupled oscillators is to “nullify” the mean field at the coupling node CN, i.e., to remove the reason of synchronization. The corresponding diagram is shown in **Figure 11**.

We repeat here Eq. (12) from Section 3 for clarity and for comparison with Eq. (30):

$$\begin{aligned}\dot{x}_i &= F(x_i) - y_i - \gamma + k(\langle x \rangle - x_i), \\ \dot{y}_i &= x_i - \beta_i y_i\end{aligned}$$

and emphasize that the mean-field value $\langle x \rangle$ by itself is not zero:

$$\langle x \rangle = \frac{1}{N} \sum_{i=1}^N x_i \neq 0. \quad (29)$$

The control technique implicates that the mean-field variable $\langle x \rangle$ is not fully nullified, but its value at the coupling node CN, $\langle x \rangle_{CN}$ is set zero:

$$\begin{aligned} \dot{x}_i &= F(x_i) - y_i - \gamma + k(0 - x_i), \\ \dot{y}_i &= x_i - \beta_i y_i. \end{aligned} \tag{30}$$

The coupling node is simply grounded, as sketched in **Figure 11**. Numerical results are shown in **Figure 12**. Note that when the control is switched on, the value of actual mean-field variable $\langle x \rangle$ becomes relatively small, but is not zero.

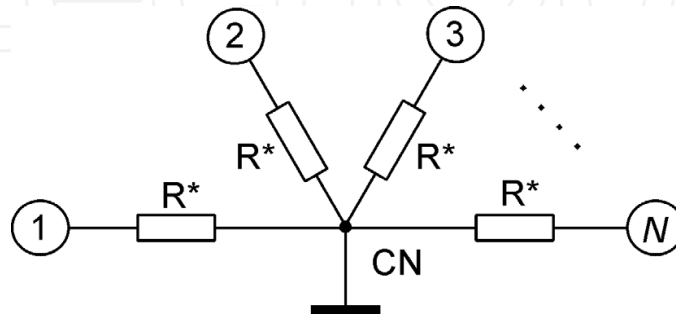


Figure 11. Diagram of mean-field coupled oscillators with the coupling node CN grounded.

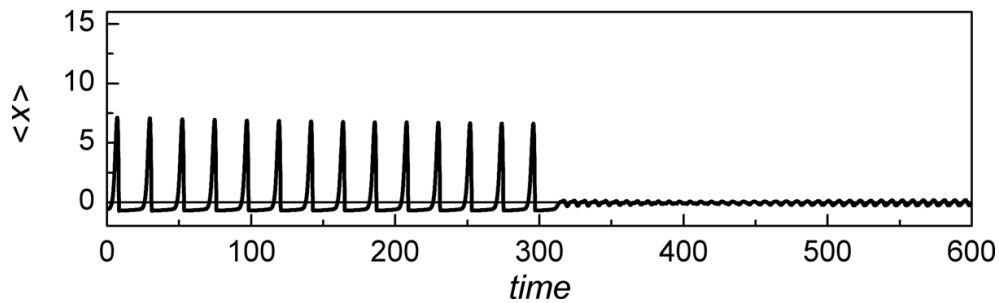


Figure 12. Waveform of the mean-field variable $\langle x \rangle$ from Eq. (30). $N = 24$, $\alpha = 1.5$, $\beta_i = 0.05 + 0.001i$, $\gamma = 1$, $\delta = 10^{-5}$, $\mu = 20$, and $k = 1$. Control is switched on at $t = 300$ ($x_{CN} = \langle x \rangle$ in the coupling term is replaced with $x_{CN} = 0$).

6. Repulsive coupling technique

An alternative method of desynchronization of coupled oscillators is the repulsive coupling, also called “repulsive synchronization” technique [26]. Diagram is sketched in **Figure 13**.

Voltage at the coupling node x_{CN} is found from the Kirchhoff’s law for current:

$$\sum_{i=1}^N k(x_i - x_{CN}) - Gx_{CN} = 0, \tag{31}$$

$$x_{CN} = \frac{V_{CN}}{V^*}, \quad G = \frac{\rho}{R_n}. \tag{32}$$

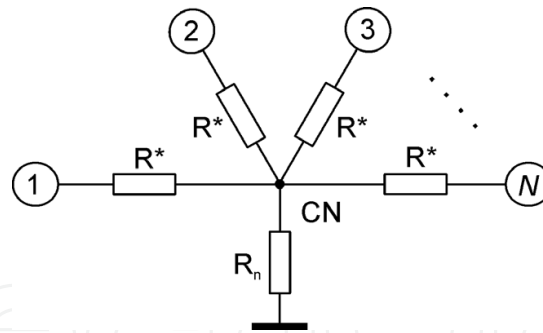


Figure 13. Diagram of mean-field coupled oscillators with coupling node CN, grounded via resistor R_n .

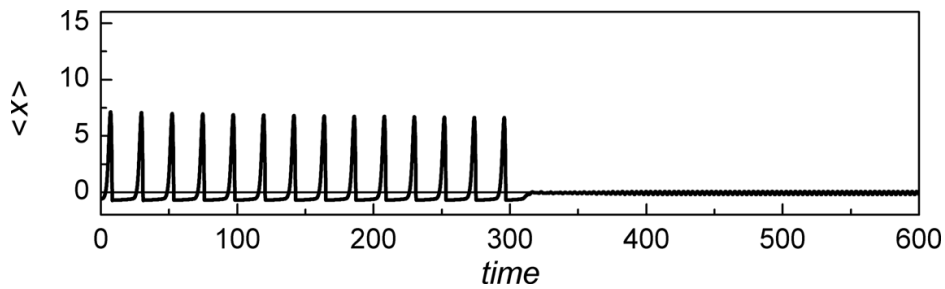


Figure 14. Waveform of the mean-field variable $\langle x \rangle$ from Eq. (34). $N = 24$, $\alpha = 1.5$, $\beta_i = 0.05 + 0.001i$, $\gamma = 1$, $\delta = 10^{-5}$, $\mu = 20$, and $k = 1$. Control is switched on at $t = 300$ ($x_{CN} = \langle x \rangle$ in the coupling term is replaced with $x_{CN} = -\langle x \rangle$).

Eq. (31) yields:

$$x_{CN} = kN\langle x \rangle / (kN + G). \tag{33}$$

Evidently, for $R_n = 0$, the $G \rightarrow \infty$ and $x_{CN} = 0$, as expected. It is the case considered in previous Section 5. If R_n is negative, say it provides value of $G = -2kN$, then $x_{CN} = -\langle x \rangle$. It is the case of so-called repulsive coupling:

$$\begin{aligned} \dot{x}_i &= F(x_i) - y_i - \gamma + k(-\langle x \rangle - x_i), \\ \dot{y}_i &= x_i - \beta_i y_i. \end{aligned} \tag{34}$$

Numerical results are presented in **Figure 14**. Similarly to the mean-field “nullifying” technique, the mean $\langle x \rangle$ becomes small, which is a typical feature of either non-synchronized or antiphase synchronized oscillators.

7. Conclusions

A modification of the FitzHugh–Nagumo (FHN) model of a spiking neuron has been proposed. In the original model, developed by FitzHugh [35], the cubic activation function $x - x^3/3$

has been replaced with a strongly asymmetric exponential one. This function provides more realistic shape of the membrane voltage spikes. Synchronization effect in an array of mean-field coupled non-identical FHN type oscillators has been demonstrated.

Three methods for controlling arrays of coupled FHN type oscillators have been described:

- Stable filter technique aimed to damp spikes in coupled oscillators. It is based on replacing the mean variable $\langle x \rangle$ at the coupling node with its filtered version z .
- Mean field nullifying technique, $\langle x \rangle = 0$ (grounding the coupling node).
- Repulsive coupling technique, following the idea described in [26] and shown for an array of Kuramoto 1D phase oscillators. It is based on replacing the mean-field variable $\langle x \rangle$ at the coupling node with the inverse version “ $-\langle x \rangle$.”

The above control techniques have different physical mechanisms behind, ranging from stabilization of the equilibrium states to desynchronization and antiphase synchronization. However, all of them ensure low value of mean-field variable in the array.

Author details

Elena Adomaitienė, Skaidra Bumelienė and Arūnas Tamaševičius*

*Address all correspondence to: arunas.tamasevicius@ftmc.lt

Department of Electronics, Center for Physical Sciences and Technology, Vilnius, Lithuania

References

- [1] Kuo BC. Automatic Control Systems. Englewood Cliffs, New Jersey: Prentice-Hall; 1995
- [2] Ogata K. Modern Control Engineering. Englewood Cliffs, New Jersey: Prentice-Hall; 2010
- [3] Rulkov NF, Tsimring LS, Abarbanel HDI. Tracking unstable orbits in chaos using dissipative feedback control. *Physical Review E*. 1994;**50**(1):314-324. DOI: 10.1103/PhysRevE.50.314
- [4] Namajūnas A, Pyragas K, Tamaševičius A. Stabilization of an unstable steady state in a Mackey–Glass system. *Physics Letters A*. 1995;**204**(3–4):255-262. DOI: 10.1016/0375-9601(95)00480-Q
- [5] Pyragas K, Pyragas V, Kiss IZ, Hudson JL. Stabilizing and tracking unknown steady states of dynamical systems. *Physical Review Letters*. 2002;**89**:244103. DOI: 10.1103/PhysRevLett.89.244103
- [6] Pikovsky A, Rosenblum M, Kurths J. Synchronization: A Universal Concept in Nonlinear Sciences. Cambridge: Cambridge University Press; 2003

- [7] Rosenblum MG, Controlling PAS. Synchronization in an ensemble of globally coupled oscillators. *Physical Review Letters*. 2004;**92**:114102. DOI: 10.1103/PhysRevLett.92.114102
- [8] Popovych OV, Hauptmann C, Effective TPA. Desynchronization by nonlinear delayed feedback. *Physical Review Letters*. 2005;**94**:164102. DOI: 10.1103/PhysRevLett.94.164102
- [9] Pyragas K, Popovych OV, Tass PA. Controlling synchrony in oscillatory networks with a separate stimulation-registration setup. *Europhysics Letters*. 2007;**80**:40002. DOI: 10.1209/0295-5075/80/40002
- [10] Ratas I, Pyragas K. Controlling synchrony in oscillatory networks via an act-and-wait algorithm. *Physical Review E*. 2014;**90**:032914. DOI: 10.1103/PhysRevE.90.032914
- [11] Bielawski S, Bouazaoui M, Derozier D, Glorieux P. Stabilization and characterization of unstable steady state in a laser. *Physical Review A*. 1993;**47**(4):3276-3279. DOI: 10.1103/PhysRevA.47.3276
- [12] Johnston GA, Hunt ER. Derivative control of the steady state in Chua's circuit driven in the chaotic region. *IEEE Transactions on Circuits and Systems*. 1993;**40**(11):833-835. DOI: 10.1109/81.251822
- [13] Parmananda P, Rhode MA, Johnson GA, Rollins RW, Dewald HD, Markworth AJ. Stabilization of unstable steady state in an electrochemical system using derivative control. *Physical Review E*. 1994;**49**(6):5007-5011. DOI: 10.1103/PhysRevE.49.5007
- [14] Namajūnas A, Pyragas K, Tamaševičius A. Analog techniques for modeling and controlling the Mackey–Glass system. *International Journal of Bifurcation and Chaos*. 1997;**7**(4):957-962. DOI: 10.1142/S0218127497000406
- [15] Ciofini M, Labate A, Meucci R, Galanti M. Stabilization of unstable fixed points in the dynamics of a laser with feedback. *Physical Review E*. 1999;**60**(1):398-402. DOI: 10.1103/PhysRevE.60.398
- [16] Schenck zu Schweinsberg A, Dressler U. Characterization and stabilization of the unstable fixed points of a frequency doubled Nd:YAG laser. *Physical Review E*. 2001;**63**(5):056210. DOI: 10.1103/PhysRevE.63.056210
- [17] Huijberts H. Linear controllers for the stabilization of unknown steady states of chaotic systems. *IEEE Transactions on Circuits and Systems I*. 2006;**53**(10):2246-2254. DOI: 10.1109/TCSI.2006.883157
- [18] Pyragas K, Pyragas V, Kiss IZ, Hudson JL. Adaptive control of unknown unstable steady states of dynamical systems. *Physical Review E*. 2004;**70**(2):026215. DOI: 10.1103/PhysRevE.70.026215
- [19] Braun DJ. Adaptive steady-state stabilization for nonlinear dynamical systems. *Physical Review E*. 2008;**78**(1):016213. DOI: 10.1103/PhysRevE.78.016213
- [20] Tamaševičius A, Tamaševičiūtė E, Mykolaitis G, Bumelienė S. Switching from stable to unknown unstable steady states of dynamical systems. *Physical Review E*. 2008;**78**(2):026205. DOI: 10.1103/PhysRevE.78.026205

- [21] Tamaševičius A, Tamaševičiūtė E, Mykolaitis G, Bumelienė S, Kirvaitis R. Stabilization of saddle steady states of conservative and weakly damped dissipative dynamical systems. *Physical Review E*. 2010;**82**(2):026205. DOI: 10.1103/PhysRevE.82.026205
- [22] Tamaševičius A, Tamaševičiūtė E, Mykolaitis G, Bumelienė S. Enhanced control of saddle steady states of dynamical systems. *Physical Review E*. 2013;**88**(3):032904. DOI: 10.1103/PhysRevE.88.032904
- [23] Tamaševičiūtė E, Mykolaitis G, Bumelienė S, Tamaševičius A. Stabilizing saddles. *Physical Review E*. 2013;**88**(6):060901(R). DOI: 10.1103/PhysRevE.88.060901
- [24] Adomaitienė E. Development of Methods for Controlling Equilibrium and Synchrony of Nonlinear Dynamical Systems [Thesis]. Vilnius: Vilnius University; 2017
- [25] Adomaitienė E, Bumelienė S, Mykolaitis G, Tamaševičius A. Stabilization of a network of the FitzHugh–Nagumo oscillators by means of a single capacitor based RC filter feedback technique. *Complexity*. 2017;**2017**:4324879. DOI: 10.1155/2017/4324879
- [26] Tsimring LS, Rulkov NF, Larsen ML, Repulsive GM. Synchronization in an array of phase oscillators. *Physical Review Letters*. 2005;**95**(1):014101. DOI: 10.1103/PhysRevLett.95.014101
- [27] Tukhlina N, Rosenblum M, Pikovsky A, Kurths J. Feedback suppression of neural synchrony by vanishing stimulation. *Physical Review E*. 2007;**75**(1):011918. DOI: 10.1103/PhysRevE.75.011918
- [28] Tamaševičiūtė E, Mykolaitis G, Tamaševičius A. Feedback controller for destroying synchrony in an array of the FitzHugh–Nagumo oscillators. *Applied Physics Letters*. 2012;**101**(22):223703. DOI: 10.1063/1.4768938
- [29] Tamaševičius A, Mykolaitis G, Tamaševičiūtė E, Bumelienė S. Two-terminal feedback circuit for suppressing synchrony of the FitzHugh–Nagumo oscillators. *Nonlinear Dynamics*. 2015;**81**(1–2):783-788. DOI: 10.1007/s11071-015-2028-y
- [30] Benabid AL, Chabardes S, Mitrofanis J, Polak P. Deep brain stimulation of the subthalamic nucleus for the treatment of Parkinson's disease. *The Lancet Neurology*. 2009;**8**(1):67-81. DOI: 10.1016/S1474-4422(08)70291-6
- [31] Pyragas K, Novičenko V, Tass PA. Mechanism of suppression of sustained neuronal spiking under high-frequency stimulation. *Biological Cybernetics*. 2013;**107**(6):669-684. DOI: 10.1007/s00422-013-0567-1
- [32] Pyragas K, Tass PA. Suppression of spontaneous oscillations in high-frequency stimulated neuron models. *Lithuanian Journal of Physics*. 2016;**56**(4):223-238. DOI: 10.3952/physics.v56i4.3419
- [33] Adomaitienė E, Mykolaitis G, Bumelienė S, Tamaševičius A. Inhibition of spikes in an array of coupled FitzHugh–Nagumo oscillators by external periodic forcing. *Nonlinear Analysis: Modelling and Control*. 2017;**22**(3):421-429. DOI: 10.15388/NA.2017.3.10

- [34] Horowitz P, Hill W. Art of Electronics. 2nd ed. Cambridge, New York, Melbourne: Cambridge University Press; 1993
- [35] FitzHugh R. Impulses and states in theoretical models of nerve. Biophysical Journal. 1961;1(6):445-466. DOI: 10.1016/S0006-3495(61)86902-6
- [36] Tamaševičius A, Tamaševičiūtė E, Mykolaitis G, Bumelienė S, Kirvaitis R, Stoop R. Neural spike suppression by adaptive control of an unknown steady state. Lecture Notes in Computer Science. 2009;5768(Part I):618-627. DOI: 10.1007/978-3-642-04274-4_64

IntechOpen